ARTICLE NO. 78-1194

Hot-Wire, Laser-Anemometer, and Force Measurements of Interacting Trailing Vortices

J. D. Iversen,* V. R. Corsiglia†
S. Park,‡ D. R. Backhus,‡ and R. A. Brickman‡
Iowa State University, Ames, Iowa

Single and multiple trailing vortices shed from semispan wings and a transport model in a wind tunnel were studied by means of a laser velocimeter, hot-wire anemometer, and trailing model incorporating a six-component force balance. Velocity profile and turbulence data from the laser velocimeter and hot-wire anemometer are presented and shown to compare well with the Betz inviscid circulation model. Lift and rolling moment measurements on the following model are compared with those predicted from the flowfield measurements.

Nomenclature

b = wing span
c = wing chord
C_L = lift coefficient
C_l = rolling moment coefficient
C_N = yawing moment coefficient
d = distance between two interacting vortices
d_0 = initial value of d
d_Γ = characteristic vortex diameter (Ref. 3)
U = mean axial velocity
U_∞ = mean freestream velocity
U_θ = mean tangential velocity
u' = axial component fluctuation velocity
u'_θ = tangential component fluctuation velocity
$\overline{u'}$ = root-mean-square axial turbulence, $(\overline{u'^2})^{1/2}$
$\overline{u'_\theta}$ = root-mean-square tangential turbulence, $(\overline{u'^2_\theta})^{1/2}$
$\overline{u'u'_\theta}$ = cross-correlation turbulent component
x = distance downstream from vortex-generating model
x_m = distance downstream to merging point
ν = kinematic viscosity
Γ = circulation in vortex
Γ_0 = large radius circulation (equal to wing centerline circulation)

Introduction

In recent years considerable research has been conducted into the problem of aircraft wake vortices. The vortices can present a hazard to closely following aircraft and thus limit aircraft spacing during landing and takeoff operations. A major part of this research has focused on modifying the generator aircraft so as to minimize the effect of the wake on following aircraft. One method of achieving this is to shed multiple corotating vortices on each wing semispan, since these multiple vortices have been shown to merge into a single diffused wake vortex.[1-4] Several efforts are underway to model these vortices theoretically using inviscid models and various models for the turbulent viscosity.[2,5,6] These efforts are hampered, however, by a lack of data on the velocity and turbulence distributions within vortices undergoing merger. There is, therefore, considerable interest in the detailed structure of the merging vortices.

Recently, flow visualization[3,4] and laser-velocimeter studies[7-9] were completed and reported in which vortex interaction and merging characteristics were studied. Measurements of velocity profiles by means of the laser velocimeter were incomplete over the vortex cross sections because of seeding problems in the vortex cores. Also, the output of the frequency tracker used with the laser velocimeter was not suitable for determination of turbulence characteristics within the vortex. A hot-wire anemometer was thus used to obtain missing mean velocity data within the vortex cores and also to obtain turbulence data. Also, a following model mounted on a force balance was placed in the vortices generated by one or two semispan wings and also in the wake of a model Boeing 747 wide-body transport. Data from the laser velocimeter not previously reported on, data taken with the hot-wire anemometer, and force-balance data from the following model are presented in this paper.

Wind-Tunnel Facility and Instrumentation

The Iowa State University (ISU) open-circuit wind tunnel has a test section cross section of 91.4 by 76.2 cm with a streamwise length extendable to 8.5 m. Low-turbulence intensity (from 0.1 to 0.2% over most of the test section) is provided by means of a large inlet to test section contraction ratio and by a series of screens at the inlet. The trailing vortices were generated by one or two semispan wings mounted on the floor and side wall of the test section at any one of four streamwise locations (see Ref. 7) or by a one-hundredth scale wide-body transport model (Boeing 747) mounted in an inverted position on the tunnel floor.

The laser velocimeter used (loaned by the NASA Ames Research Center) is a two-color (blue and green), two-component system using an argon-ion laser. The instrument is described in detail in Refs. 7 and 8. The hot-wire anemometer used is a Thermo-Systems 1050 model. A two-wire crossed-wire boundary layer probe (to minimize interference) was used for most of the hot-wire experiments. The boundary layer probe is curved so that when the wire are near the vortex center, the only portion of the probe close to the core is that portion near the wires. Most of the probe is perpendicular to the stream outside the vortex core and downstream from the wires. A six-component internal strain-gage force balance was used for force measurements on the following model. Characteristics of the model are listed in the appendix.

Vortex Meander

The lateral excursions to which a trailing vortex is prone when situated in a stream containing ambient turbulence has

Presented as Paper 78-1194 at the AIAA 11th Fluid and Plasma Dynamics Conference, Seattle, Wash., July 10-12, 1978; received Oct. 16, 1978.

Index categories: Aerodynamics; Jets, Wakes, and Viscid-Inviscid Flow Interactions.

*Professor, Dept. of Aerospace Engineering, Iowa State University. Associate Fellow AIAA.

†Aerospace Engineer, NASA Ames Research Center. Member AIAA.

‡Research Assistant, Iowa State University.

long caused problems in measurement of vortex characteristics.[10] Reed[11] shows that meander amplitude is linearly proportional both to the level of freestream turbulence and to the downstream distance from the generating lifting surface. In the low-turbulence wind tunnel, the meander amplitude is reduced because of the reduction in stream turbulence. In the case of the laser measurements, a technique was devised to reduce the effects of meander still further. The wind-tunnel flow was seeded with a mineral oil aerosol to provide scattering material for the laser velocimeter. A light slit, illuminating the oil mist, was used to mark a lateral plane just downstream of the laser measurement plane so that the vortex center location could be continually monitored and data sampled only when the vortex center was in a prescribed location. The conditional sampling technique was not possible for the hot-wire measurements, since the hot wire must operate in a particle-free environment. The reasonably good agreement, however, between laser and hot-wire measurements leads to some degree of confidence in the validity of the hot-wire results.

Hot-Wire Anemometer Data

The two-wire crossed-wire probe was used to measure axial and tangential components of the mean and fluctuation velocities in the vortex cross-section planes. The laser-anemometer data are considered to be freer from error than the hot-wire data for the following reasons: 1) the laser instrument does not require calibration; 2) the effect of vortex meander was minimized by conditional sampling using a flow visualization technique; and 3) probe interference was absent. The sampling technique was not possible for the hot-wire measurements. An additional disadvantage of the hot-wire technique is that the wire is sensitive primarily to only that velocity component normal to the wire and in the plane containing the wire and the total velocity vector. Thus, in order to be able to use the two-wire probe to measure velocity in a known direction, it is necessary to orient the plane of the probe in a direction tangent to a stream surface. The plane in which data can be taken is thus limited, for example, to the vertical plane for a vertically oriented probe, and for an axisymmetric vortex to one line of data on a horizontally oriented probe.

Some of the hot-wire data are shown in Figs. 1-8. Figure 1 illustrates data for a vortex trailing from a single wing. The mean axial and tangential velocities are shown in Figs. 1a and b and the turbulent components $\overline{u'}/U_\infty$ (longitudinal); $\overline{u'_\theta}/U_\infty$(tangential), and $\overline{u'u'_\theta}/\overline{u'}\,\overline{u'_\theta}$ are illustrated in Figs. 1c-e for $x/b=3.25$ and $\Gamma_0/U_\infty b=0.0903$. The tangential velocity profile from data taken farther downstream at $x/b=8.49$ is illustrated in Fig. 2. Some comments concerning the shapes of the turbulent energy curves are in order. Bilanin et al.,[12] with their second-order turbulence closure model, predict that the centrifugal effect of the swirling velocity in a vortex is to suppress turbulent energy completely for equilibrium, nondiffusive, high-Reynolds-number limit conditions in the inner region of a Lamb vortex. Donaldson's calculations[13] of the decay of a Lamb vortex using the same turbulence closure model shows that while turbulence energy is not suppressed to zero at the vortex center, sufficient suppression takes place so that an initial vortex distribution with maximum turbulent energy in the vortex center is modified in the near downstream to a distribution with maximum energy in an annular region surrounding the center. Farther downstream the energy distribution in his calculation levels off to a nearly constant value in the vortex core. The annular peak region of turbulent kinetic energy also appears experimentally in Singh and Uberoi's data.[14] At $x/b=3.46$, they show turbulent energy of 2% at a radius-to-chord ratio r/c of 0.05 and only 1% at the vortex center. In the current tests, at $x/b=3.25$, the maximum energy appears at the vortex center. The difference between the current tests and Singh and Uberoi's is probably due to the difference in swirl strength.

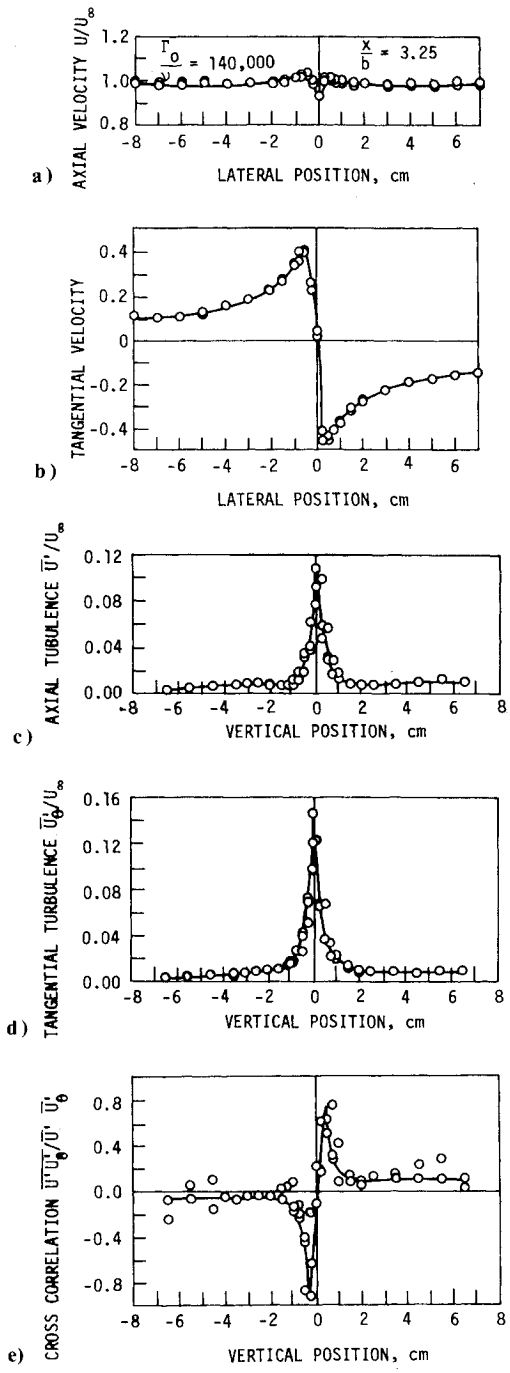

Fig. 1 Hot-wire anemometer data for a single-wing trailing vortex, $x/b=3.25$: a) axial speed distribution; b) tangential speed distribution; c) axial turbulence distribution; d) tangential turbulence distribution; e) cross-correlation distribution.

Their peak tangential velocity at $x/b=3.46$ is 54% of the freestream speed, while in the current tests the peak tangential speed is only 42% at $x/b=3.25$. Also the inviscid vorticity distribution in the current tests is less concentrated due to the difference in generator planform shape. Farther downstream in Singh and Uberoi's data, where the peak tangential speed has decayed to 40% at $x/b=11.11$, the maximum turbulent energy is at the vortex center, as in the current tests. The effects of vortex meander are difficult to assess, and may be such as to blur the annular energy peak if one exists. The authors are not sure that such blurring has not taken place, but they do not believe that it has at $x/b=3.25$.

Both mean and fluctuating maximum velocities have decayed somewhat with downstream distance. The rate of decay and the corresponding rate of increase of core radius

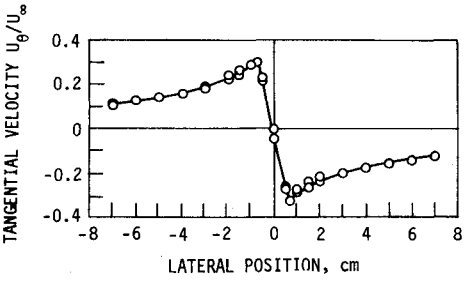

Fig. 2 Hot-wire anemometer data for a single-wing trailing vortex, $x/b = 8.49$, tangential speed distribution.

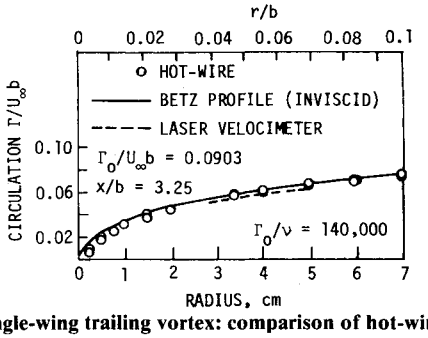

Fig. 3 Single-wing trailing vortex: comparison of hot-wire and laser-velocimeter data with inviscid Betz circulation profile.

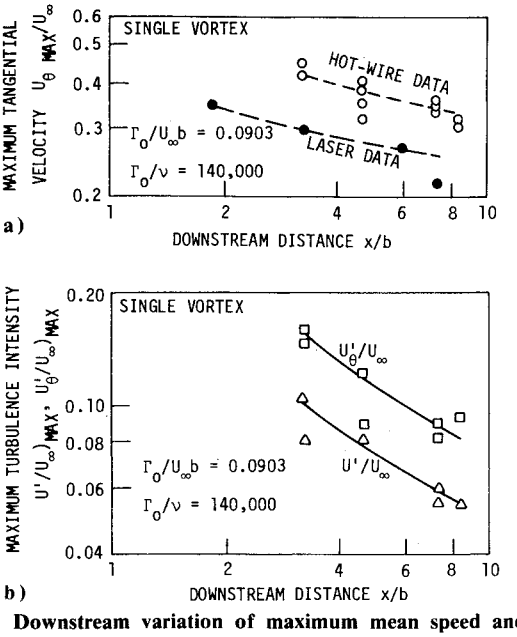

Fig. 4 Downstream variation of maximum mean speed and turbulence data for the single-wing trailing vortex; a) streamwise decay of maximum tangential speed—comparison of hot-wire and laser-velocimeter data; b) streamwise decay of maximum and tangential turbulent components.

are small, however. The excellent agreement between hot-wire data, laser data, and the inviscid Betz theory[15] is illustrated in Fig. 3. The decay with downstream distance is illustrated in Fig. 4. These data points lie within the plateau region,[16] and so the decay of maximum tangential speed is less than as the inverse square root of the downstream distance. That the peak values were not reached by the laser velocimeter because of lack of seeding material in the vortex core is apparent from Fig. 4a. Figure 4b illustrates the decay of peak tangential and axial fluctuation velocities with downstream distance. Some of the data scatter in these curves may be due to variations in the freestream turbulence level and/or the effects of vortex meander.

Hot-wire traverses for two interacting vortices at $x/b = 3.25$ are shown in Fig. 5. The locations of the two vortices, the hot-wire traverse paths, and the tangential velocity profile along the vertical traverse of vortex 1 are illustrated in Fig. 5a, while the profile along the horizontal traverse path of vortex 2 is shown in Fig. 5b.

Figure 6 illustrates the hot-wire mean velocity and turbulence data for a merged vortex. The mean axial and tangential velocity data are shown in Figs. 6a and b. Superimposed on the tangential velocity data are the data from the laser anemometer. The agreement is relatively good. The turbulence data are presented in Figs. 6c-e. Finally, a comparison of the single-vortex and merged-vortex tangential velocity profiles is depicted in Fig. 6f. The merged vortex contains twice as much large radius circulation as does the single vortex; yet the peak tangential speed is even lower than for the single vortex. Very little decay has taken place, apparently, during the merging process, since the core of the merged vortex has nearly the same diameter as that for the single vortex.

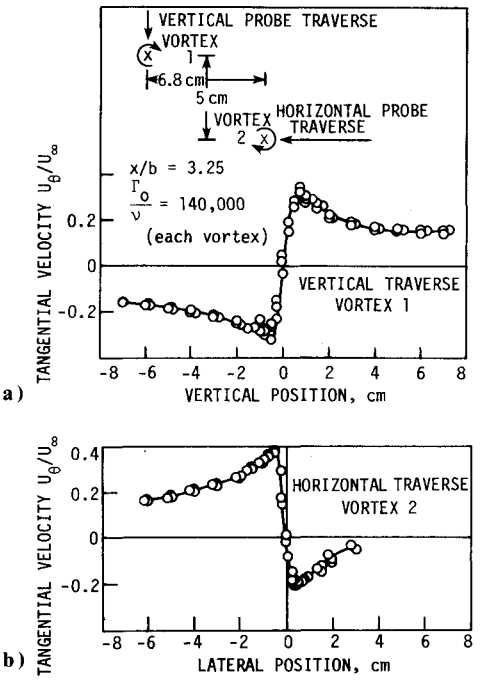

Fig. 5 Hot-wire data for two interacting vortices $x/b = 3.25$; a) tangential speed distribution—vortex 1, vertical traverse; b) tangential velocity distribution—vortex 2, horizontal traverse.

Laser Velocimeter Data for the Model Transport

The final experiment with the laser velocimeter involved the survey of the wake of the model of the Boeing 747 transport aircraft. The laser survey plane was located a distance of 1.33 m downstream of the model ($x/b = 2.23$). Several methods of hazard reduction have been tried both in ground-based experiments and in full-scale flight tests.[17] Methods that have been shown to reduce significantly the hazard to trailing aircraft (reduction of induced rolling moment) include unconventional flap deflection,[17] unconventional spoiler deployment,[18] and the use of a lifting surface fin deployed on the wing upper surface.[19] The model used in the laser velocimeter was equipped with deployable leading- and trailing-edge flaps and landing gear. Spoilers and the upper surface fin could also be attached to the model.

Results for the conventional landing configuration at landing lift coefficient ($C_L = 1.2$) are shown in Fig. 7. For the conventionally loaded wing with full leading- and trailing-edge flaps, the wing loading is close to elliptic, and most of the visible wake (visible via the seeding material introduced at

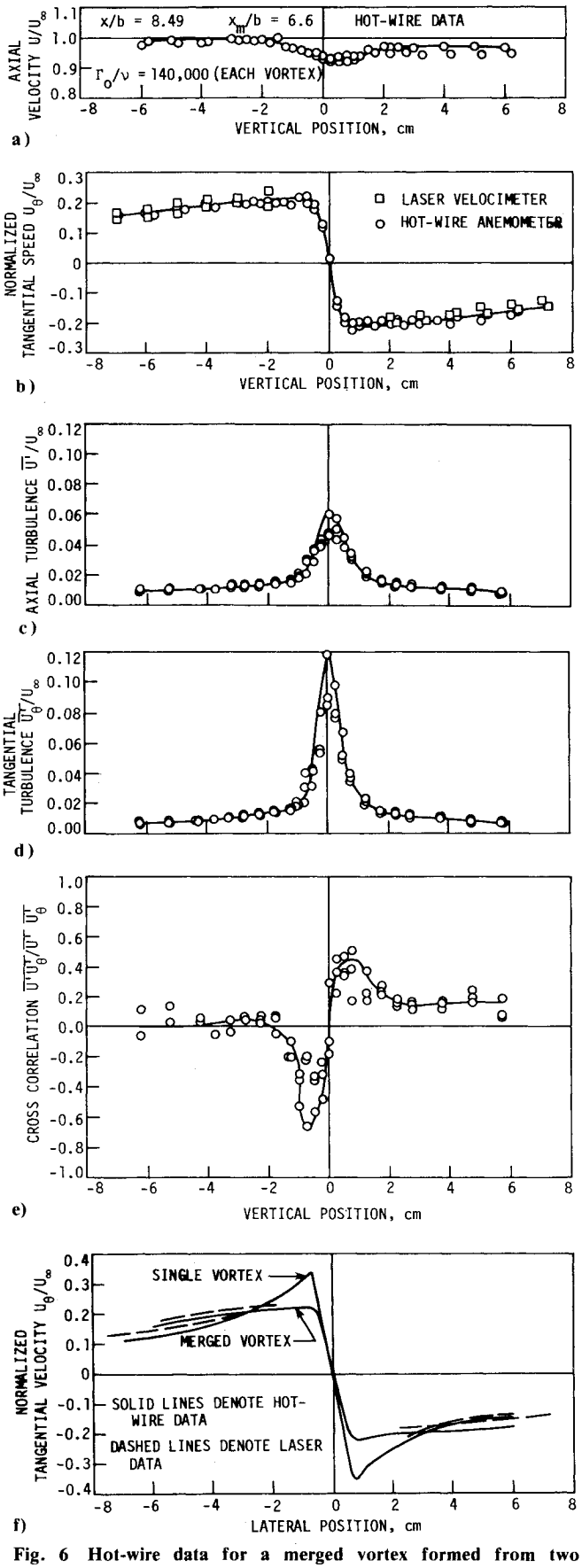

Fig. 6 Hot-wire data for a merged vortex formed from two corotating equal-strength vortices, $x/b = 8.49$: a) axial speed distribution; b) tangential speed distribution—comparison of hot-wire and laser data; c) axial turbulence distribution; d) tangential turbulence distribution; e) cross-correlation turbulence distribution; f) comparison of single-vortex and merged-vortex tangential speed distributions with hot-wire and laser-velocimeter data.

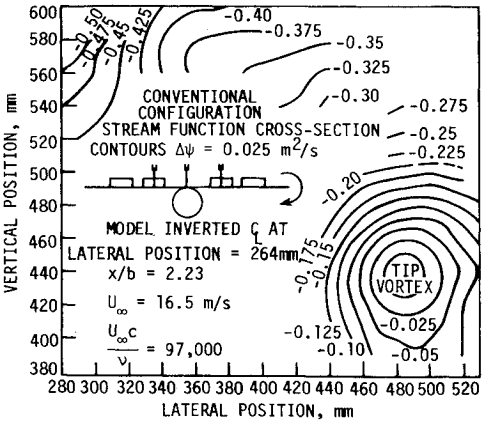

Fig. 7 Laser-velocimeter data for Boeing 747 1/100 scale transport model, $x/b = 2.23$, conventional landing configuration, stream-function cross-section contours.

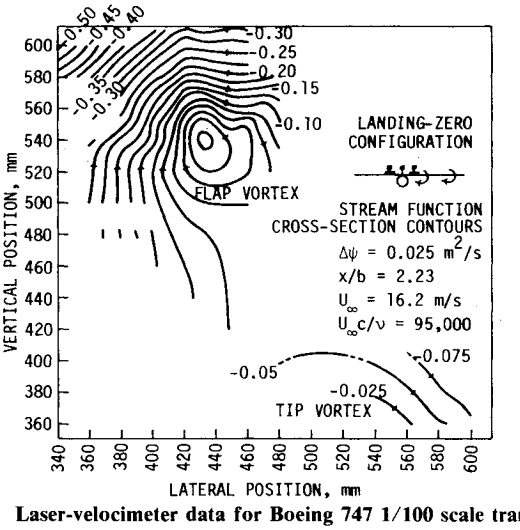

Fig. 8 Laser-velocimeter data for Boeing 747 1/100 scale transport model, $x/b = 2.23$, landing-zero configuration (inboard flap deployed normally, outboard flap retracted), stream-function cross-section contours.

the tunnel inlet) is wrapped up in the large tip vortex region at the lower right in Fig. 7.

Figure 8 illustrates the landing-zero configuration, in which the outboard set of flaps are retracted and the angle of attack increased to obtain the same lift coefficient. In this case the primary vortex is that shed from the outboard edge of the deployed inboard flap. Later downstream this vortex merges with the weaker tip vortex and presents a reduced hazard to following aircraft compared to the conventionally loaded wing.

Results for the upper surface fin are somewhat more difficult to interpret. Flow visualization showed that the strong vortex shed from the fin on the otherwise conventionally loaded wing quickly merged with the vortex shed from the outboard edge of the inboard flap. This vortex then, in turn, may have merged with the outboard flap and tip vortices. It was difficult to ascertain the merging sequence from the flow visualization because turbulence diffused the smoke rapidly in the wake of the wing. At any rate, the stream-function cross-section contours in Fig. 9 do not reveal a complete discrete vortex, although there appear to be two centers of vorticity of opposite sign located at the lower right and upper left. The vorticity has been greatly diffused from the conventional loading by the fin. Results for the spoiler case are inconclusive. So much turbulence was introduced by the spoilers that the seeding material was diffused to the extent that only a very small portion of the flowfield could be measured.

Table 1 Force and moment coefficient results and capability for the following model

Force coefficient	Typical follower control capability	Range of induced coefficients on follower		
		Conventional generator	Landing-zero flaps	Upper surface fin
Roll, C_l	±0.05	−0.125 to +0.095	−0.05 to +0.11	−0.04 to +0.055
Pitch, $C_{m_{1/4}}$	−0.35 to +0.60	−0.20 to +0.10	−0.40 to +0.60	−0.20 to +0.90
Lift, C_L	−0.22 to +0.13	−0.40 to +0.40	−0.40 to +0.50	0 to +0.60
Yaw, C_N	±0.032	−0.20 to +0.10	−0.04 to +0.06	−0.03 to +0.04
Side force, C_Y	±0.061	−0.08 to +0.11	−0.11 to +0.08	−0.03 to +0.08

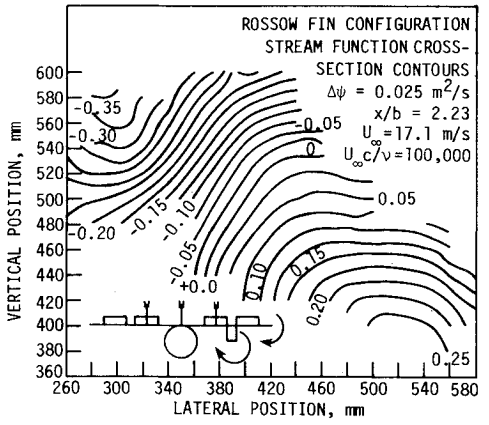

Fig. 9 Laser-velocimeter data for Boeing 747 1/100 scale transport model, $x/b = 2.23$, Rossow fin configuration (upper surface fin), stream function cross-section contours.

Force Balance Experiments

A following model, consisting of an aspect ratio 5.2 rectangular wing, was placed at a distance of 2.35 m ($x/b = 3.94$) downstream of the 747 model and various distances downstream of the two semispan wing models ($x/b = 3.25$ to 8.49). The following model wing and its relative size are representative of a Learjet type of aircraft. All six components of force and moment were measured. Some of the results of these experiments are presented in Figs. 10 and 11. Figure 10a presents rolling moment coefficient contours obtained from the merged vortex with the two semispan models mounted 6.15 m ($x/b = 8.49$) upstream of the force-balance model. The merging point was estimated as 1.6 m upstream of the following model. Figure 10b presents rolling moment contours for two semispan wings mounted only 2.35 m upstream. The merging distance in this case is estimated to be 2.0 m downstream of the following model. From rolling moment contours (not shown) for the 747 model as generator with the conventional upper surface fin and landing-zero configurations, the upper surface fin presents considerably reduced maximum rolling moment over a much reduced area than does the conventional configuration.

Although the rolling moment coefficient has been considered the best quantitative indicator of hazard to a following aircraft, and rightfully so, the lift coefficient is also of prime importance in evaluating follower response. The induced lift coefficient can vary by a factor of 1 from one portion of the wake to another. The upper surface fin is again the best 747 configuration because the total lift coefficient variation (0.6) is the least for that model.

The effect of vortex merging on follower hazard is more dramatically depicted in Fig. 11. Figure 11a shows the rolling moment coefficient on the following model as evaluated from lifting line theory as a function of lateral position in the vortex. The experimental tangential velocity profiles for a single vortex (Fig. 2) and for the merged vortex (Fig. 6b) were used in the lifting-line analysis. Although the merged vortex contains twice as much large-radius circulation, generated

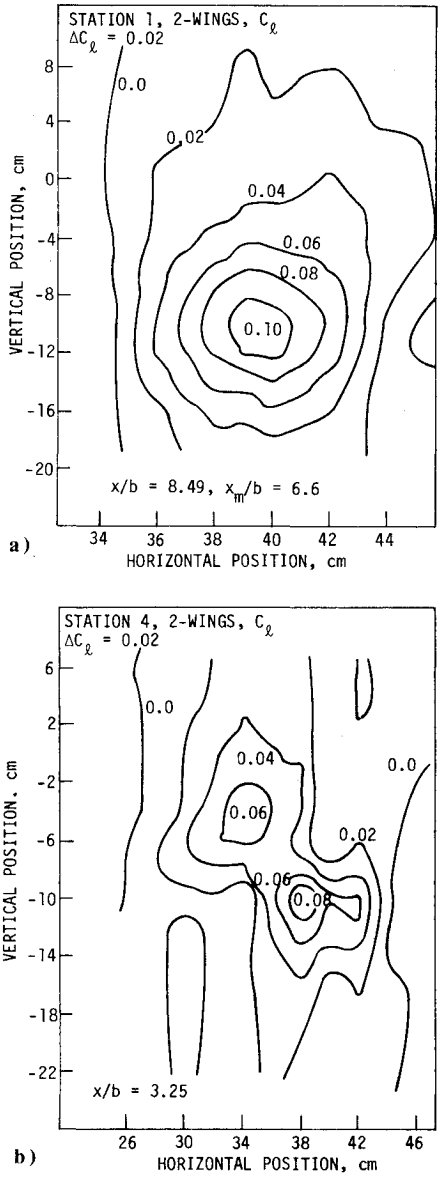

Fig. 10 Rolling moment coefficient on following model ($b = 11.59$ cm, $c = 2.22$ cm): a) model situated in merged vortex 8.49 generator spans downstream of two semispan wings ($b = 72.4$ cm); b) model situated in interacting vortex field 3.25 generator spans downstream of two semispan wings ($b = 72.4$ cm).

with twice as much lift as the single vortex, because of the diffusion of vorticity in the merged vortex, the rolling moment coefficient calculated from the two cases is almost identical, indicating a relative hazard due to the merged vortex of only 50% of that from a single trailing vortex.

The merged vortex rolling moment coefficient is replotted in Fig. 11b along with the experimental data from the following model. The agreement is good except for the larger

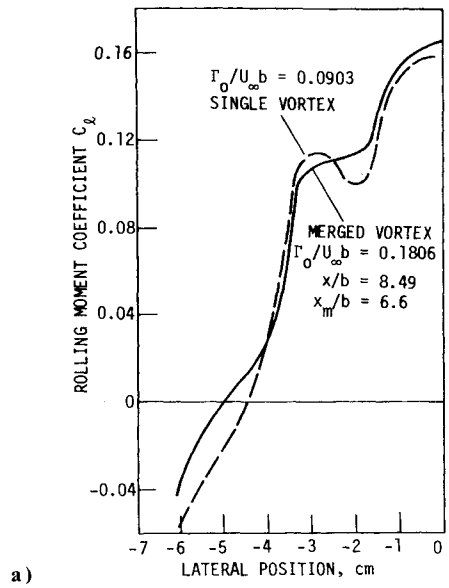

a)

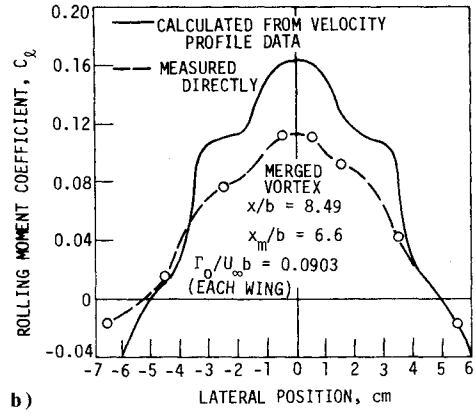

b)

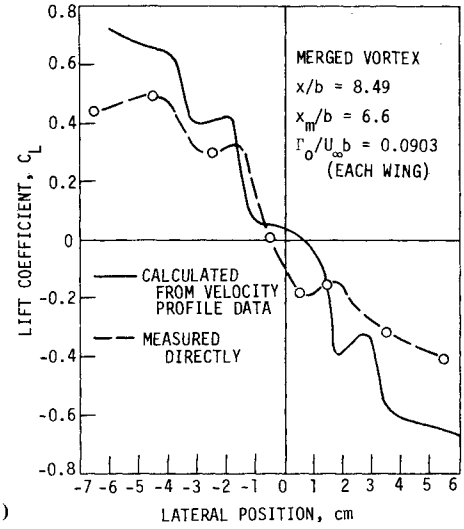

c)

Fig. 11 Rolling moment and lift coefficient on the following model as a function of lateral position with respect to the center of the merged vortex ($x/b = 8.49$, generator spans = 72.4 cm): a) rolling moment coefficient for single and merged trailing vortices calculated from hot-wire velocity profiles; b) rolling moment coefficient for merged trailing vortex—comparison of values calculated from hot-wire data with values measured; c) lift coefficient for merged trailing vortex—comparison of values calculated from hot-wire data with values measured.

values of induced rolling moment. The lifting-line analysis did not account for the possibility of local stall on the following model, which probably accounts for most of the difference, although it may also be partly due to the distortion of the vortex as the air flows over the model (the core diameter and wing chord are about the same value). The calculated and measured values of lift coefficients are shown in Fig. 11c as a function of lateral position of the following model. Again, the agreement is relatively good, with better agreement for smaller values of the lift coefficient. The calculated values of yawing moment and drag coefficients are not as reliable because these values rely on predicted values of local drag. The experimental local drag variation on the model is likely to differ a good bit from the theoretical induced drag variation because of the low Reynolds number of the following model (approximately 50,000).

The peak values of coefficients induced on the follower by the three 747 configurations are tabulated in Table 1, along with the maximum control capability of a Learjet-sized airplane. In most cases, the only generator configuration for which the follower would have sufficient or nearly surfficient counteracting control capability is the upper surface fin configuration. The follower in the current tests was located only 3.94 generator spans downstream (0.15 miles equivalent full scale), and the relative hazard conditions will change with distance downstream. Larger scale tests at a greater downstream distance, however, have shown that the upper surface fin configuration has resulted in the lowest induced rolling moment coefficients of all variations tried thus far.[19]

Conclusions

Hot-wire anemometer data are found to be in good agreement with previously obtained laser-velocimeter data in spite of the effects of probe interference and vortex meander. Thus, the measurements of turbulence reported here are believed to be reliable. The turbulence data show that for the single vortex, the axial and tangential components of turbulent energy decay in about the same manner with downstream distance as the peak tangential mean speed.

The merged vortex, formed from the interaction of two equal-strength corotating vortices, shows a peak tangential speed lower than that of the single vortex at the same downstream distance, although it contains twice as much large-radius circulation and has about the same core diameter. The turbulent energy contained within the vortex is about four times as great as for a single vortex, indicating that the merging process is responsible for turbulent energy production and resultant diffusion of vorticity outward for the merged vortex.

Laser-velocimeter data obtained in the wake of a 747 model transport are presented in the forms of stream-function contours. These data show strong vortices associated with the tip vortex for the conventional landing configuration, and with the inboard flap vortex for the landing-zero configuration. The upper surface vortex-generating fin, or Rossow fin, appears to diffuse the wake vorticity to the extent that the follower rolling moment coefficient is significantly reduced from that induced from the conventional landing configuration. Yawing moment and lift coefficients induced on the follower by the merged vortex and the various 747 configurations are also presented.

Appendix—Model Characteristics

1) Semispan wing models consisted of a 15.24-cm chord wing with a NACA 0012 airfoil section. The outboard 10.16 cm of the span consisted of an elliptical chord distribution.[9]

2) The heavy transport model was mounted with a swept strut protruding from the upper rather than lower surface of the fuselage in order to minimize interaction of vortices emanating from the strut-fuselage juncture with all the other vortices generated on the basic model. The model was

equipped with removable leading- and trailing-edge flaps, spoilers, and landing gear. The wing span is 59.7 cm, the area 511 cm^2, and the aspect ratio 6.96.

3) The following model consisted of an axisymmetric center body, an NACA 0012 airfoil section, and a rectangular planform of 11.59-cm span and 2.22-cm chord for an aspect ratio of 5.21.

Acknowledgments

This research is supported by the NASA Ames Research Center and by the Engineering Research Institute, Iowa State University.

References

[1] Corsiglia, V.R., Rossow, V.J., and Ciffone, D.L., "Experimental Study of the Effect of Span Loading on Aircraft Wakes," *Journal of Aircraft*, Vol. 13, Dec. 1976, pp. 968-973.

[2] Rossow, V.J., "Convective Merging of Vortex Cores in Lift-Generated Wakes," *Journal of Aircraft*, Vol. 14, March 1977, pp. 283-290.

[3] Brandt, S.A. and Iversen, J.D., "Merging of Aircraft Trailing Vortices," *Journal of Aircraft*, Vol. 14, Dec. 1977, pp. 1212-1220.

[4] Iversen, J.D., Brandt, S.A., and Raj, P., "Merging Distance Criteria for Co-Rotating Trailing Vortices," *Proceedings of U.S. Dept. of Transportation Conference on Aircraft Wake Vortices*, Cambridge, Mass., March 1977.

[5] Bilanin, A.J., Teske, M.E., and Williamson, G.G., "Vortex Interactions and Decay in Aircraft Wakes," *AIAA Journal*, Vol. 15, Feb. 1977, pp. 250-260.

[6] Raj, P. and Iversen, J.D., "Computational Studies of Turbulent Merger of Co-Rotational Vortices," presented as Paper 78-108 at the AIAA 16th Aerospace Sciences Meeting, Huntsville, Ala., Jan. 16-18, 1978.

[7] Corsiglia, V.R., Iversen, J.D., and Orloff, K.L., "Laser-Velocimeter Surveys of Merging Vortices in a Wind Tunnel," *Journal of Aircraft*, Vol. 15, Nov. 1978, pp. 762-768.

[8] Corsiglia, V.R., Iversen, J.D., and Orloff, K.L., "Laser-Velocimeter Surveys of Merging Vortices in a Wind Tunnel—Complete Data and Analysis," NASA Ames Research Center, NASA TM X-78449, April 1978.

[9] Iversen, J.D. and Corsiglia, V.R., "The Role of Turbulence in Vortex Wake Decay," Iowa State University, ISU-ERI-Ames-77393, 1977.

[10] Corsiglia, V.R., Schwind, R.G., and Chigier, N.A., "Rapid-Scanning Three-Dimensional, Hot-Wire Anemometer Surveys of Wing-Tip Vortices," *Journal of Aircraft*, Vol. 10, Dec. 1973, pp. 752-757.

[11] Reed, R.E., Jr., "Properties of the Lateral Random Oscillations of Trailing Vortices Observed in Wind Tunnel Tests," Nielsen Engineering, NEAR TR-47, Jan. 1973.

[12] Bilanin, A.J., Teske, M.E., Donaldson, C. duP., and Snedeker, S.R., "Viscous Effects in Aircraft Trailing Vortices," *Proceedings of NASA Symposium on Wake Vortex Minimization*, Washington, D.C., NASA SP-409, Feb. 1976, pp. 61-128.

[13] Donaldson, C. duP., "Calculation of Turbulent Shear Flows for Atmospheric and Vortex Motions," *AIAA Journal*, Vol. 10, 1972, pp. 4-12.

[14] Singh, P.I. and Uberoi, M.S., "Experiments on Vortex Stability," *Physics of Fluids*, Vol. 19, Dec. 1976, pp. 1858-1863.

[15] Rossow, V.J., "On the Inviscid Rolled-Up Structure of Lift Generated Vortices," *Journal of Aircraft*, Vol. 10, Nov. 1973, pp. 647-650.

[16] Cliffone, D. and Orloff, K., "Far Field Wake Vortex Characteristics of Wings," *Journal of Aircraft*, Vol. 12, May 1975, pp. 464-470.

[17] Corsiglia, V.R. and Dunham, R.E. Jr., "Aircraft Wake-Vortex Minimization by Use of Flaps," *Proceedings of NASA Symposium on Wake Vortex Minimization*, Washington, D.C., NASA SP-409, Feb. 1976, pp. 303-336.

[18] Croom, D.R., "Low-Speed Wind Tunnel Investigation of Various Segments of Flight Spoilers as Trailing Vortex Alleviation Devices on Transport Aircraft Model," NASA Langley Research Center, NASA TN D-8162, March 1976.

[19] Rossow, V.J., "Effect of Wing Fins on Lift-Generated Wakes," *Journal of Aircraft*, Vol. 15, March 1978, pp. 160-167.